

Probing the alignment of NO ($X^2\Pi$) by [2+1] resonance-enhanced multiphoton ionization via the $C^2\Pi$ state: A test of semiclassical theory in 355 nm photodissociation of NO 2

Yuxiang Mo, Hideki Katayanagi, and Toshinori Suzuki

Citation: *The Journal of Chemical Physics* **110**, 2029 (1999); doi: 10.1063/1.477849

View online: <http://dx.doi.org/10.1063/1.477849>

View Table of Contents: <http://scitation.aip.org/content/aip/journal/jcp/110/4?ver=pdfcov>

Published by the **AIP Publishing**

Articles you may be interested in

Erratum: "Photodissociation dynamics of 3-bromo-1,1,1-trifluoro-2-propanol and 2-(bromomethyl) hexafluoro-2-propanol at 234 nm: Resonance-enhanced multiphoton ionization detection of Br ($2P_j$)" [*J. Chem. Phys.* **134**, 194313 (2011)]

J. Chem. Phys. **135**, 029902 (2011); 10.1063/1.3610529

Photodissociation dynamics of 3-bromo-1,1,1-trifluoro-2-propanol and 2-(bromomethyl) hexafluoro-2-propanol at 234 nm: Resonance-enhanced multiphoton ionization detection of Br ($2P_j$)

J. Chem. Phys. **134**, 194313 (2011); 10.1063/1.3591373

Photodissociation and photoionization of 2,5-dihydroxybenzoic acid at 193 and 355 nm

J. Chem. Phys. **133**, 244309 (2010); 10.1063/1.3518709

Photoionization and photodissociation dynamics of H₂ after (3+1) resonance-enhanced multiphoton ionization via the $B^1\Sigma_u^+$ state

J. Chem. Phys. **109**, 8319 (1998); 10.1063/1.477495

The $\tilde{A}^2\Sigma^+$ state of ArNO studied using resonance-enhanced multiphoton and zero-kinetic-energy pulsed-field ionization spectroscopy

J. Chem. Phys. **108**, 406 (1998); 10.1063/1.475402



Probing the alignment of $\text{NO}(X^2\Pi)$ by $[2+1]$ resonance-enhanced multiphoton ionization via the $C^2\Pi$ state: A test of semiclassical theory in 355 nm photodissociation of NO_2

Yuxiang Mo, Hideki Katayanagi, and Toshinori Suzuki^{a)}
Institute for Molecular Science, Myodaiji, Okazaki 444-8585, Japan

(Received 3 April 1998; accepted 13 October 1998)

A theoretical method to analyze the two- and three-dimensional imaging data of photofragments with polarized angular momentum was tested by comparing with the experimental data on NO from 355 nm photodissociation of NO_2 . The alignment of $\text{NO}(X^2\Pi)$ was detected by $[2+1]$ resonance-enhanced multiphoton ionization via the $C^2\Pi$ state. The data were analyzed by assuming the $\boldsymbol{\mu}-\boldsymbol{\nu}-\mathbf{J}$ triple vector correlation described by semiclassical multipole moments in the *velocity-fixed* frame. The geometrical factors for the two-photon absorption were derived rigorously for the intermediate coupling between Hund's cases (a) and (b). It was also shown, however, that the geometrical factors for high J are independent of the coupling case and can be approximated by simple formulas. Excellent agreement between the simulation and the experimental data proved the validity of the semiclassical treatment. © 1999 American Institute of Physics.
[S0021-9606(99)00203-2]

I. INTRODUCTION

Vector correlation among the absorption dipole moment ($\boldsymbol{\mu}$), the product recoil velocity ($\boldsymbol{\nu}$), and the product angular momentum (\mathbf{J}) provides detailed insights into the stereodynamics in photodissociation.¹⁻¹⁴ Similar correlation among the relative velocity vectors before and after the collision (\mathbf{k} and \mathbf{k}'), and the product angular momentum (\mathbf{J}) are also important in atomic and molecular collision dynamics.¹⁵⁻¹⁷

In the 1980s state-resolved scattering distributions of photofragments were measured by one-dimensional (1D) Doppler spectroscopy.¹⁻⁸ However, more recently, two-dimensional (2D)^{9-12,18} and three-dimensional (3D) ion-imaging methods¹⁹⁻²¹ became much more powerful experimental means for this purpose. The first observation of the $\boldsymbol{\nu}-\mathbf{J}$ correlation by the ion-imaging technique was reported by Houston and co-workers for $\text{O}_2(a^1\Delta)$ from photodissociation of O_3 .¹⁰ However, rigorous theoretical treatment of the vector correlation in ion-imaging experiments has not been established yet.

This work reports a semiclassical formalism to treat the vector correlation and its critical test by comparison with the experimental data on NO from photodissociation of NO_2 . The angular momentum polarization of NO is expressed by the multipole moments in the *velocity-fixed* (VF) frame.¹³ It is noted that one, two, and k photon absorption processes provide the multipole moments only up to the rank 2, 4, and $2k$, meaning that full determination of the multipole moments is practically impossible for a diatomic fragment. However, in photodissociation of triatomic molecule, conservation of helicity leads to a simple $\boldsymbol{\nu}\perp\mathbf{J}$ correlation in the diatomic fragment (for high J), which allows us to describe

multipole moments semiclassically with only three parameters.

Photodissociation of NO_2 at 355 nm has been extensively studied.²¹⁻²⁵ However, the vector correlation in NO photofragment has not been observed by $[1+1]$ REMPI (resonance-enhanced multiphoton ionization) via the $A(^2\Sigma)$ state.^{21,23} As an alternative approach, the present work employs $[2+1]$ REMPI via the $C(^2\Pi)$ state.

II. EXPERIMENT

A supersonic beam of NO_2 was generated using a pulsed valve (0.8 mm ϕ) and two skimmers (0.5 mm ϕ). The molecular beam 1 mm in diameter was introduced parallel to the electric field vector of a time-of-flight mass spectrometer through the second skimmer embedded in the repeller plate.²¹ The concentration of NO_2 seeded in He was 5%. The stagnation pressure was 1000 Torr relative to the vacuum.

The molecular beam intersected with the counterpropagated photolysis (355 nm) and probe laser beams at 79 mm downstream from the nozzle. Both laser beams were focused by axisymmetric lenses ($f=300$ mm for photolysis and $f=250$ mm for probe). The time delay between the photolysis and probe laser pulses was kept within 20 ns by a digital delay generator. NO was probed by $[2+1]$ REMPI via the $C^2\Pi_y(j=30.5, f)$ state using the $Q_{y1,ff}(30.5)$ line²⁶⁻²⁸ ($52\,612.3\text{ cm}^{-1}$). We determined the energy levels of the $C^2\Pi$ state by combining the experimental data previously reported.²⁶⁻³⁰ $\text{O}(^3P_0)$ was probed by $[2+1]$ REMPI via the $3p\ ^3P$ state around 226 nm. Since the absorption lines are broadened by Doppler effect due to the recoil velocities, the probe laser frequency was scanned over the entire Doppler-broadened absorption lines during the integration of ion images.

The photofragment ions were accelerated and projected

^{a)}Electronic mail: suzuki@ims.ac.jp

onto a microchannel plate (effective diameter 38 mm) backed by a phosphor screen (P20). Ten ring-shaped electrodes were used to generate the acceleration field with 2D space focusing effect.¹⁸ At the time when NO⁺ arrived at the microchannel plate (MCP), a high voltage pulse 1700–1800 V in height and 200–500 ns in duration was applied to the MCP, raising the gain up to 10⁶–10⁷. Thus, the signals due to the scattered light of laser beams and background ions with different masses were discriminated. The high voltage pulse was generated by a homemade power supply using a transistor switch. The transient image on the phosphor screen was captured by a thermoelectrically cooled charge-coupled device (CCD) camera. Typical background pressures in the beam source and the main chamber were 2 × 10⁻⁵ Torr and 2 × 10⁻⁷ Torr, respectively, when the pulsed valve was operated. The photolysis and probe laser polarization directions were rotated independently by double Fresnel rhombs.

III. THEORY

A. Absorption intensity of linearly and circularly polarized light

When an optical method is used to detect atoms or molecules with a density matrix ρ , the signal intensity can be expressed as follows:^{31–37}

$$I = c \text{Tr}(\hat{O}\rho) = c \sum_{M_i M'_i} \langle n_i J_i M_i | \hat{O} | n_i J_i M'_i \rangle \rho_{M'_i M_i}, \quad (1)$$

where Tr means the trace of the matrix, and $|n_i J_i M_i\rangle$ describes a quantum state with rotational quantum number J_i , magnetic quantum number M_i , and all other quantum numbers represented by n_i . \hat{O} is the operator for the optical transition, and c is a constant. For instance, the matrix element for one-photon absorption process is given by³¹

$$\langle n_i J_i M_i | \hat{O} | n_i J_i M'_i \rangle = \sum_{M_f} \langle n_f J_f M_f | \vec{r} \cdot \hat{\epsilon} | n_i J_i M_i \rangle^* \langle n_f J_f M_f | \vec{r} \cdot \hat{\epsilon} | n_i J_i M'_i \rangle. \quad (2)$$

The subscript f indicates the states reached by absorption. \vec{r} is the dipole moment operator and $\hat{\epsilon}$ is the unit vector for the electric field of the light. For linearly or circularly polarized light, the polarization direction \mathbf{E} (linearly polarized light) or the propagation direction \mathbf{k} (circularly polarized light) can be chosen as the z^{PR} axis (probe laser photon fixed frame; PR frame). Then, the operator in Eq. (2) is expressed by

$$\vec{r} \cdot \hat{\epsilon} = (-1)^s r_s^{(1)} \epsilon_{-s}^{(1)}, \quad (3)$$

where $s=0$ for linearly polarized light and $s=\pm 1$ for circularly polarized light. $r_s^{(1)}$ and $\epsilon_s^{(1)}$ are the spherical basis.³³ Then, Eq. (2) is transformed into

$$\langle n_i J_i M_i | \hat{O} | n_i J_i M'_i \rangle = \delta_{M_i, M'_i} \sum_{M_f} \langle n_f J_f M_f | r_s^{(1)} | n_i J_i M_i \rangle^* \times \langle n_f J_f M_f | r_s^{(1)} | n_i J_i M'_i \rangle. \quad (4)$$

The matrix elements for multiphoton absorption can be obtained similarly.

Thus, Eq. (1) is expressed by

$$\begin{aligned} I &= c \text{Tr}(\hat{O}\rho) = c \sum_{M_i} \langle n_i J_i M_i | \hat{O} | n_i J_i M_i \rangle \rho_{M_i M_i} \\ &= c \sum_{M_i} \langle n_i J_i M_i | \hat{O} | n_i J_i M_i \rangle \sum_k \\ &\quad (-1)^{J_i - M_i} \sqrt{2k+1} \\ &\quad \times \begin{pmatrix} J_i & k & J_i \\ -M_i & 0 & M_i \end{pmatrix} \rho_0^{(k)}(\text{PR}) \end{aligned} \quad (5a)$$

$$= c \sum_k P_k \rho_0^{(k)}(\text{PR}), \quad (5b)$$

where

$$\rho_{M_i M_i} = \sum_k (-1)^{J_i - M_i} \sqrt{2k+1} \begin{pmatrix} J_i & k & J_i \\ -M_i & 0 & M_i \end{pmatrix} \rho_0^{(k)}(\text{PR}), \quad (6a)$$

$$\begin{aligned} P_k &= \sum_{M_i} \langle n_i J_i M_i | \hat{O} | n_i J_i M_i \rangle (-1)^{J_i - M_i} \sqrt{2k+1} \\ &\quad \times \begin{pmatrix} J_i & k & J_i \\ -M_i & 0 & M_i \end{pmatrix}. \end{aligned} \quad (6b)$$

$\rho_0^{(k)}(\text{PR})$ in Eq. (6a) are the multipole moments in the PR frame. P_k in Eq. (6b) are called *geometrical* factors which depend on the number of photons absorbed and the type of the transition.

Because of the cylindrical symmetry in the PR frame, the absorption intensity is only sensitive to the zero components of the multipole moments (in other words, the diagonal elements of the density matrix).³²

In practical applications, it is convenient to use the multipole moment in an arbitrary *space-fixed* (SF) coordinate. If the polar angles of the z^{PR} axis in the SF coordinate are (θ_p, ϕ_p) , the multipole moments in the two frames are related as follows:³²

$$\begin{aligned} \rho_0^{(k)}(\text{PR}) &= \sum_q \rho_q^{(k)}(\text{SF}) D_{q0}^{(k)*}(\phi_p, \theta_p, 0) \\ &= \sum_q \rho_q^{(k)}(\text{SF}) C_{kq}(\theta_p, \phi_p), \end{aligned} \quad (7)$$

where $D_{q0}^{(k)}(\phi_p, \theta_p, 0)$ is the Wigner rotation matrix and $C_{kq}(\theta_p, \phi_p)$ is the modified spherical harmonics. Inserting Eq. (7) into Eq. (5b), the following general formula for absorption intensity is obtained:

$$I = c \sum_k P_k \sum_q \rho_q^{(k)}(\text{SF}) C_{kq}(\theta_p, \phi_p). \quad (8)$$

It is seen from Eq. (8) that the expression for the signal intensity is separated into three parts, (1) the geometrical factors P_k that are calculated from Eq. (6b), (2) the multipole moments $\rho_q^{(k)}(\text{SF})$, and (3) the angular relation between the PR and SF frames.

B. Geometrical factors P_k for two-photon transition

Kummel *et al.*³⁴ and Docker³⁵ provided the geometrical factors P_k for two-photon transition in diatomic molecules in the pure Hund's case (a). Here we consider the diatomic molecules in the intermediate coupling between the Hund's cases (a) and (b).

1. General formula for the intermediate coupling between Hund's cases (a) and (b)

By using Eq. (6b) and the two-photon absorption formula,³⁴ the geometrical factors can be derived as follows:

$$P_k = \sum_{M_i M_f} \left| \sum_{J_e M_e} \sum_{n_e} \frac{\langle n_f J_f M_f | \vec{r} \cdot \hat{\epsilon} | n_e J_e M_e \rangle \langle n_e J_e M_e | \vec{r} \cdot \hat{\epsilon} | n_i J_i M_i \rangle^2}{E_{n_e J_e} - E_i - i\Gamma_{n_e J_e}/2 - h\nu} \right| \times (-1)^{J_i - M_i} \sqrt{2k+1} \begin{pmatrix} J_i & k & J_i \\ -M_i & 0 & M_i \end{pmatrix}. \quad (9)$$

The subscripts f , e , and i represent the final, virtual and initial states, respectively. $\Gamma_{n_e J_e}$ is the total homogeneous width of the virtual state.

In the intermediate coupling case between the Hund's cases (a) and (b), the wave functions of the initial and final states are expanded by the Hund's case (a) basis,

$$|n_i J_i M_i\rangle = \sum_{\Omega} C_{\Omega}^{(i)} \psi(2S+1 \Lambda_{\Omega=\Sigma+\Lambda})_i, \quad (10a)$$

$$|n_f J_f M_f\rangle = \sum_{\Omega} C_{\Omega}^{(f)} \psi(2S+1 \Lambda_{\Omega=\Sigma+\Lambda})_f, \quad (10b)$$

where $\psi(2S+1 \Lambda_{\Omega=\Sigma+\Lambda})_i$ and $\psi(2S+1 \Lambda_{\Omega=\Sigma+\Lambda})_f$ represent the basis functions in Hund's case (a) for the initial and the

final states. $C_{\Omega}^{(i)}$ and $C_{\Omega}^{(f)}$ are the corresponding expansion coefficients, respectively. Λ and Σ denote the projections of orbital and spin angular momenta onto the molecular axis, respectively. For instance, in the case of $X^2\Pi$ and $C^2\Pi$ of NO, Eqs. (10a) and (10b) are described more explicitly as follows:³³

$$|X, J_i M_i\rangle = c_{1/2}^{(i)} |X^2\Pi_{1/2}\rangle + c_{3/2}^{(i)} |X^2\Pi_{3/2}\rangle, \quad (10c)$$

$$|C, J_f M_f\rangle = c_{1/2}^{(f)} |C^2\Pi_{1/2}\rangle + c_{3/2}^{(f)} |C^2\Pi_{3/2}\rangle. \quad (10d)$$

As shown in Appendix A, Eq. (9) can be simplified as follows:

$$P_k = (-1)^{J_f + J_i} (2J_f + 1) \sqrt{2k+1} \sum_{RT} X^{(R)} X^{(T)*} Y^{(R)} Y^{(T)*} \times \begin{pmatrix} 1 & 1 & R \\ s & s & -2s \end{pmatrix} \begin{pmatrix} 1 & 1 & T \\ s & s & -2s \end{pmatrix} \begin{pmatrix} R & T & k \\ 2s & -2s & 0 \end{pmatrix} \times \begin{Bmatrix} J_i & J_i & k \\ T & R & J_f \end{Bmatrix}, \quad (11a)$$

where

$$X^{(R)} = \sum_{\Omega_f \Omega_i} (-1)^{J_i - \Omega_i} \sqrt{2J_i + 1} \times \begin{pmatrix} J_i & R & J_f \\ -\Omega_i & \Omega_i - \Omega_f & \Omega_f \end{pmatrix} C_{\Omega_i}^{(i)} C_{\Omega_f}^{(f)*}, \quad (11b)$$

$$Y^{(R)} = \sum_{\Lambda_e} (2R + 1) \times \begin{pmatrix} 1 & 1 & R \\ \Lambda_f - \Lambda_e & \Lambda_e - \Lambda_i & \Lambda_i - \Lambda_f \end{pmatrix} G(\Lambda_e), \quad (11c)$$

$$G(\Lambda_e) = \sum_{n_e} \frac{\langle n_f \Lambda_f S \Sigma | r_{\Lambda_f - \Lambda_e}^{(1)} | n_e \Lambda_e S \Sigma \rangle \langle n_e \Lambda_e S \Sigma | r_{\Lambda_e - \Lambda_i}^{(1)} | n_i \Lambda_i S \Sigma \rangle}{E_{n_e \Lambda_e} - E_i - i\Gamma_{n_e \Lambda_e}/2 - h\nu}. \quad (11d)$$

The notation $Y^{(R)}$ corresponds to $\sqrt{2R+1} T_k^{(R)}$ by Meyer.³⁶

2. Simple cases

It can be seen from Eqs. (11a)–(11c) that, in the following cases, only the $R=T=2$ term is nonzero:

- (i) the circularly polarized light,
- (ii) the linearly polarized light with $J_i \neq J_f$,
- (iii) the linearly polarized light with $J_i = J_f$ and $\Lambda_i \neq \Lambda_f$.

Therefore, in these cases, the relative values of geometrical factors are given by

$$P_k/P_0 = 5 \sqrt{2k+1} \sqrt{2J_i+1} (-1)^{J_i+J_f} \begin{pmatrix} 2 & 2 & k \\ 2s & -2s & 0 \end{pmatrix} \times \begin{Bmatrix} J_i & J_i & k \\ 2 & 2 & J_f \end{Bmatrix}. \quad (12)$$

This simple relation has been obtained by Docker for the pure Hund's case (a) with linearly polarized light ($s=0$).³⁵ However, this is generally valid for atoms and molecules in the above cases (i) and (ii).³⁷ In Sec. III B 3, the special case of $J_i = J_f$ and $\Lambda_i = \Lambda_f$ is considered.

3. A special case: Linearly polarized light with $J_i = J_f$ and $\Lambda_i = \Lambda_f$

In this case, R and T of 0 or 2 provide nonzero values in the summation in Eq. (11a). From Eq. (11c), we obtain

$$Y^{(R)} = (2R+1) \begin{pmatrix} 1 & 1 & R \\ -1 & 1 & 0 \end{pmatrix} [G(\Lambda_i-1) + G(\Lambda_i+1)] + (2R+1) \begin{pmatrix} 1 & 1 & R \\ 0 & 0 & 0 \end{pmatrix} G(\Lambda_i). \quad (13)$$

Therefore, the ratio between perpendicular and parallel (\perp ||) transitions, $[G(\Lambda_i - 1) + G(\Lambda_i + 1)] : G(\Lambda_i)$, must be known to calculate $P_0 : P_2 : P_4$. [If the transition involves $^{2S+1}\Sigma_0$ state, special attention should be paid to $G(\Lambda_e)$, see Appendix A.] $G(\Lambda_e)$ can be determined experimentally or computationally.

Equation (11b) shows that the relative geometrical factors depend generally on the coupling cases in the initial and final states. However, if J_i is large, such consideration becomes unnecessary. For $R=0$, Eq. (11b) is simplified as

$$X^{(0)} = \sum_{\Omega} C_{\Omega}^{(i)} C_{\Omega}^{(f)*}. \quad (14)$$

For $R=2$ and $J_i \gg \Omega_i$, the 3- j symbol in Eq. (11b) can be approximated by

$$(-1)^{J_i - \Omega_i} \sqrt{2J_i + 1} \begin{pmatrix} J_i & 2 & J_i \\ -\Omega_i & 0 & \Omega_i \end{pmatrix} \approx -\frac{1}{2}, \quad (15a)$$

$$(-1)^{J_i - \Omega_i} \sqrt{2J_i + 1} \begin{pmatrix} J_i & 2 & J_i \\ -\Omega_i & \pm 1 & \Omega_f \end{pmatrix} \approx 0. \quad (15b)$$

Here we do not consider the cases in which $\Sigma_i - \Sigma_f = \pm 2$ or the spin quantum numbers $S \geq 2$. For large J_i , therefore,

$$X^{(2)} \approx -\frac{1}{2} \sum_{\Omega} C_{\Omega}^{(i)} C_{\Omega}^{(f)*}. \quad (16)$$

Thus, the relative values of geometrical factors can be obtained by using the following values in Eq. (11a):

$$X^{(0)} = 1, \quad X^{(2)} = -0.5. \quad (17)$$

C. Signal intensity in 3D experiments

1. General formula

We define the dissociation laser photon fixed frame (DI frame) by choosing the Z^{DI} axis along the polarization direction of the dissociation laser (\mathbf{E}_{diss}). Using the recoil velocity direction as the z axis of the *molecule-fixed* frame (VF frame), the quantal form of the multipole moments in the DI frame is expressed by¹³

$$\rho_q^{(k)}(\theta_t, \phi_t) = \frac{1}{4\pi} \left(g_k C_{kq}^*(\theta_t, \phi_t) + 2 \sum_{q_2} g(k, q_2) \times D_{q-q_2}^{(k)}(\phi_t, \theta_t, 0) D_{0q_2}^{(2)}(\phi_t, \theta_t, 0) \right) \quad (18a)$$

$$= \frac{1}{4\pi} \left(g_k C_{kq}(\theta_t, 0) + 2 \sum_{q_2} g(k, q_2) \times d_{q-q_2}^{(k)}(\theta_t) d_{0q_2}^{(2)}(\theta_t) \right) e^{-iq\phi_t} \quad (18b)$$

$$= \tilde{\rho}_q^{(k)}(\theta_t) e^{-iq\phi_t}, \quad (18c)$$

where (θ_t, ϕ_t) are the polar angles of the recoil velocity in the DI frame. g_k and $g(k, q_2)$ are the expansion coefficients that represent the vector correlation in the VF frame and are defined as

$$g_k = \langle T_{k0}^+(\text{VF}) \rangle_{J'\mu'} = \int \rho_0^{(k)}(\text{VF}) d\omega'_{\mu}, \quad (18d)$$

$$g(k, q_2) = \langle T_{k-q_2}^+(\text{VF}) C_{2q_2}^*(\theta'_{\mu}, \phi'_{\mu}) \rangle_{J'\mu'} \\ = \int \rho_{-q_2}^{(k)}(\text{VF}) C_{2q_2}^*(\theta'_{\mu}, \phi'_{\mu}) d\omega'_{\mu}, \quad (18e)$$

where $T_{kq}(\text{VF})$ and $\rho_q^{(k)}(\text{VF})$ are the state multipoles and the multipole moments in the VF frame, respectively. In general, $\rho_q^{(k)}(\text{VF})$ are the functions of the transition dipole moment direction $(\theta'_{\mu}, \phi'_{\mu})$ in the VF frame.¹³ The following relation was used in obtaining Eq. (18b) from Eq. (18a);

$$D_{mn}^{(k)}(\phi, \theta, \chi) = e^{-im\phi} d_{mn}^{(k)}(\theta) e^{-in\chi}. \quad (19)$$

In Eq. (18c) we defined a new quantity $\tilde{\rho}_q^{(k)}(\theta_t)$ that we may call reduced multipole moments. It is independent of the choice of X axis in the DI frame. $\tilde{\rho}_q^{(k)}(\theta_t)$ can be expressed in an equivalent form as follows:¹³

$$\tilde{\rho}_q^{(k)}(\theta_t) = \frac{1}{4\pi} \left[C_{kq}(\theta_t, 0) g_k + 2 \sum_{q_2 k_2} (2k_2 + 1) \begin{pmatrix} 2 & k & k_2 \\ 0 & q & -q \end{pmatrix} \times \begin{pmatrix} 2 & k & k_2 \\ q_2 & -q_2 & 0 \end{pmatrix} C_{k_2 - q}(\theta_t, 0) g(k, q_2) \right]. \quad (20)$$

Since the multipole moment $\rho_q^{(k)}(\theta_t, \phi_t)$ has the following property³² (see Appendix B for the proof),

$$\rho_q^{(k)*}(\theta_t, \phi_t) = (-1)^q \rho_{-q}^{(k)}(\theta_t, \phi_t). \quad (21)$$

the reduced multipole moment has a similar relation:

$$\tilde{\rho}_q^{(k)*}(\theta_t) = (-1)^q \tilde{\rho}_{-q}^{(k)}(\theta_t). \quad (22a)$$

Another property of $\tilde{\rho}_q^{(k)}(\theta_t)$ also should be noted,

$$\tilde{\rho}_q^{(k)}(\pi - \theta_t) = (-1)^{k-q} \tilde{\rho}_q^{(k)*}(\theta_t). \quad (22b)$$

Now we turn to the calculation of the signal intensity for linearly or circularly polarized probe laser light. It is noted that the angle ϕ_t in $\rho_q^{(k)}(\theta_t, \phi_t)$ is defined relative to the X

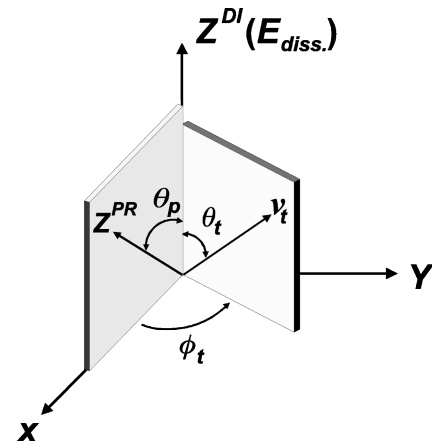


FIG. 1. Dissociation laser photon fixed frame (DI) employed in the calculation of signal intensity. The Z^{DI} axis is along the electric vector of linearly polarized dissociation laser. The symmetry axis of the probe laser (z^{PR} axis of the PR frame) lies in the XZ plane. Hence, z^{PR} axis is at polar angles $(\theta_p, 0)$. The polar angles for the recoil velocity are (θ_t, ϕ_t) .

axis of the DI frame, and the choice of X axis is arbitrary. For the convenience of calculation, we define that the X axis is in the plane formed by the polarization direction of the dissociation laser beam (Z^{DI} axis) and the symmetry axis of the probe laser beam (z^{PR} axis) (see Fig. 1). Using Eq. (22a), we simplify Eq. (8) as follows:

$$\begin{aligned}
 I(\theta_t, \phi_t) &= c \sum_k P_k \sum_q \rho_q^{(k)}(\theta_t, \phi_t) C_{kq}(\theta_p, 0) \\
 &= c \sum_k P_k \left(\tilde{\rho}_0^{(k)}(\theta_t) C_{k0}(\theta_p, 0) \right. \\
 &\quad \left. + \sum_{q>0} (\tilde{\rho}_q^{(k)}(\theta_t) C_{kq}(\theta_p, 0) e^{-iq\phi_t} \right. \\
 &\quad \left. + \tilde{\rho}_{-q}^{(k)}(\theta_t) C_{k-q}(\theta_p, 0) e^{iq\phi_t} \right) \\
 &= c \sum_k P_k \left(\tilde{\rho}_0^{(k)}(\theta_t) C_{k0}(\theta_p, 0) \right. \\
 &\quad \left. + 2 \sum_{q>0} C_{kq}(\theta_p, 0) \text{Re}(e^{-iq\phi_t} \tilde{\rho}_q^{(k)}(\theta_t)) \right), \tag{23a}
 \end{aligned}$$

where $\text{Re}(\dots)$ represents the real part of the function. For $\theta_p=0$, Eq. (8) becomes

$$I(\theta_t, \phi_t) = c \sum_k P_k \tilde{\rho}_0^{(k)}(\theta_t) \quad (\theta_p=0). \tag{23b}$$

Equations (23a) and (23b) are the basic expressions for the signal intensity in 3D imaging experiments. The reduced multipole moments are expressed by g_k and $g(k, i)$ that are more essential in describing the vector correlation in the *velocity-fixed* frame. When using linearly polarized light, two-photon absorption can determine the following coefficients:

$$g_2, g_4; \quad g(0,0), g(2,i), \quad g(4,i) \quad i=0,1,2, \tag{24}$$

where g_2 and g_4 represent the $\mathbf{v}-\mathbf{j}$ two-vector correlation, $g(0,0)$ is related with the anisotropy parameter β , and $g(2,i)$ and $g(4,i)$ represent the $\boldsymbol{\mu}-\mathbf{v}-\mathbf{j}$ triple-vector correlation. When circularly polarized light is used, the signal intensity is sensitive to both the odd and even ranks of the multipole moments, so that all the coefficients g_k and $g(k, i)$ up to $k=4$ can be determined by two-photon absorption.

When \mathbf{J} is much larger than unity and only the low ranks of multipole moments are detected, the expansion coefficients defined in Eqs. (18d) and (18e) can be approximated semiclassically as follows:

$$g_k = \sqrt{\frac{2k+1}{2J+1}} \langle P_k(\cos \theta'_j) \rangle_{J', \mu'}, \tag{25a}$$

$$\begin{aligned}
 g(k, q_2) &= \sqrt{\frac{2k+1}{2J+1}} \langle C_{k-q_2}^*(\theta'_j, \phi'_j) C_{2q_2}^*(\theta'_\mu, \phi'_\mu) \rangle_{J', \mu'} \\
 &= \sqrt{\frac{2k+1}{2J+1}} \langle C_{k-q_2}(\theta'_j, 0) C_{2q_2}(\theta'_\mu, 0) \rangle_{J', \mu'} \\
 &\quad \times e^{iq_2(\phi'_j - \phi'_\mu)} \tag{25b}
 \end{aligned}$$

where (θ'_j, ϕ'_j) and (θ'_μ, ϕ'_μ) are the polar angles of \mathbf{J} and $\boldsymbol{\mu}$ in the VF frame, respectively. The symbol $\langle \dots \rangle_{J', \mu'}$ denotes the average of the functions inside with the polar angles as integration variables.¹³ The x axis of the VF frame is chosen in the plane defined by $\boldsymbol{\mu}$ and \mathbf{v} for the convenience of calculation. The azimuthal angle of the dipole moment, ϕ'_μ , is always zero in this convention.

It is interesting to note that the multipole moments at the recoil direction (θ_t, ϕ_t) are generally different from those at $(\pi - \theta_t, \phi_t)$ and $(\theta_t, 2\pi - \phi_t)$, although the flux of the fragments for these directions are the same. We consider the polarization direction of dissociation laser perpendicular to the symmetry axis of the probe laser ($\mathbf{E}_{\text{diss}} \perp \mathbf{z}^{\text{PR}}$), i.e. $\theta_p = \pi/2$ in Eq. (23a). $C_{kq}(\pi/2, 0)$ are nonzero only when $k-q$ are even integers. Using Eqs. (22b) and (23a), the differences of the signal intensities are

$$\begin{aligned}
 I(\theta_t, \phi_t) - I(\pi - \theta_t, \phi_t) &= 2c \sum_{q>0, k} P_k C_{kq}(\pi/2, 0) \text{Re}((\tilde{\rho}_q^{(k)}(\theta_t) - \tilde{\rho}_q^{(k)*}(\theta_t)) e^{-iq\phi_t}) \\
 &= 4c \sum_{q>0, k} P_k C_{kq}(\pi/2, 0) \text{Im}(\tilde{\rho}_q^{(k)}(\theta_t)) \sin q\phi_t. \tag{26}
 \end{aligned}$$

$$\begin{aligned}
 I(\theta_t, \phi_t) - I(\theta_t, 2\pi - \phi_t) &= 2c \sum_{q>0, k} P_k C_{kq}(\theta_p, 0) \text{Re}((e^{-iq\phi_t} - e^{iq\phi_t}) \tilde{\rho}_q^{(k)}(\theta_t)) \\
 &= 4c \sum_{q>0, k} P_k C_{kq}(\theta_p, 0) \text{Im}(\tilde{\rho}_q^{(k)}(\theta_t)) \sin q\phi_t, \tag{27}
 \end{aligned}$$

where $\text{Im}(\dots)$ represents the imaginary part of the function.

Equations (26) and (27) show that the probability distributions of the projection of fragment angular momentum onto the X or Y axes are not equal for the recoil directions (θ_t, ϕ_t) and $(\pi - \theta_t, \phi_t)$ or (θ_t, ϕ_t) and $(\theta_t, 2\pi - \phi_t)$. (Another way of the explanation is given in Appendix C.)

Similar effects on the Doppler profiles resulting from the nonexistence of symmetry plane in the molecule-fixed frame, or chirality, have been discussed previously.^{6,7} The discussion presented above, however, is simpler. It is also seen clearly that the configuration, $\mathbf{E}_{\text{diss}} \perp \mathbf{z}^{\text{PR}}$, in 3D and 2D experiments provide an easy way to probe this property.

The following relations are also useful for calculating 2D images for the configuration $\mathbf{E}_{\text{diss}} \perp \mathbf{z}^{\text{PR}}$,

$$\begin{aligned}
 I(\theta_t, \phi_t) + I(\pi - \theta_t, \phi_t) &= I(\theta_t, 2\pi - \phi_t) + I(\pi - \theta_t, 2\pi - \phi_t) \tag{28a}
 \end{aligned}$$

$$= 2c \sum_k P_k \left[\tilde{\rho}_0^{(k)}(\theta_t) C_{k0}(\pi/2, 0) + 2 \sum_{q>0} C_{kq}(\pi/2, 0) \text{Re}(\tilde{\rho}_q^{(k)}(\theta_t)) \cos q \phi_t \right]. \quad (28b)$$

2. Formulas for the photodissociation with a symmetrical plane in the VF frame

If the xz plane is a symmetry plane in the VF frame, under our convention, the probability of finding the angle ϕ'_j and $-\phi'_j$ are equal, the expansion coefficients can be simplified as follows:

$$\begin{aligned} \tilde{g}(k, q_2) &= \sqrt{\frac{2k+1}{2J+1}} \langle C_{k-q_2}(\theta'_j, 0) C_{2q_2}(\theta'_{\mu'}, 0) \\ &\quad \times \cos q_2 \phi'_j \rangle_{J' \mu'}, \end{aligned} \quad (29a)$$

$$\tilde{g}_k = \sqrt{\frac{2k+1}{2J+1}} \langle P_k(\cos \theta'_j) \rangle_{J' \mu'}. \quad (29b)$$

It means that the expansion coefficients are real numbers. Therefore, for the configuration $\mathbf{E}_{\text{diss}} \perp \mathbf{z}^{\text{PR}}$, using Eqs. (26) and (27), we obtain

$$I(\pi - \theta_t, \phi_t) = I(\theta_t, \phi_t). \quad (30a)$$

$$I(\theta_t, \phi_t) = I(\theta_t, 2\pi - \phi_t). \quad (30b)$$

Noting that

$$\tilde{g}(k, q_2) = \tilde{g}(k, -q_2), \quad (31)$$

and Eq. (18b), the reduced multipole moment is calculated as follows:

$$\begin{aligned} \tilde{\rho}_q^{(k)}(\theta_t) &= \frac{1}{4\pi} \left(C_{kq}(\theta_t, 0) \tilde{g}_k + 2d_{q0}^{(k)}(\theta_t) C_{20}(\theta_t, 0) \tilde{g}(k, 0) \right. \\ &\quad + 2 \sum_{q_2=1,2} C_{2q_2}(\theta_t, 0) (d_{qq_2}^{(k)}(\theta_t) + (-1)^q \\ &\quad \times d_{-qq_2}^{(k)}(\theta_t)) \tilde{g}(k, q_2) \left. \right). \end{aligned} \quad (32)$$

Equation (32) can be written in another equivalent form by using Eqs. (20) and (31), as follows:

$$\begin{aligned} \tilde{\rho}_q^{(k)}(\theta_t) &= \frac{1}{4\pi} \left[C_{kq}(\theta_t, 0) \tilde{g}_k + 2 \sum_{k_2} (2k_2 + 1) \begin{pmatrix} 2 & k & k_2 \\ 0 & q & -q \end{pmatrix} \right. \\ &\quad \times \begin{pmatrix} 2 & k & k_2 \\ 0 & 0 & 0 \end{pmatrix} C_{k_2-q}(\theta_t, 0) \tilde{g}(k, 0) + 2 \\ &\quad \times \sum_{\substack{q_2=1,2 \\ k_2=0,1,\dots}} (1 + (-1)^{k+k_2}) (2k_2 + 1) \begin{pmatrix} 2 & k & k_2 \\ 0 & q & -q \end{pmatrix} \\ &\quad \left. \times \begin{pmatrix} 2 & k & k_2 \\ q_2 & -q_2 & 0 \end{pmatrix} C_{k_2-q}(\theta_t, 0) \tilde{g}(k, q_2) \right]. \end{aligned} \quad (33)$$

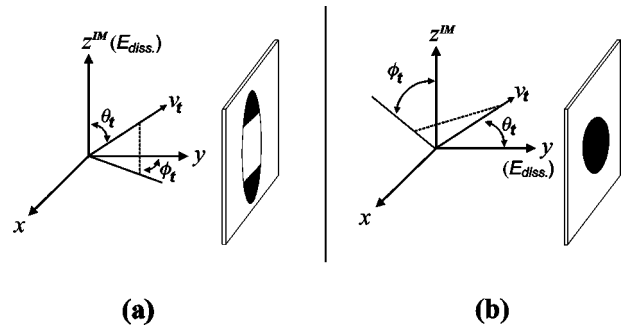


FIG. 2. Imaging frame (IM) and the polar angles of (θ_t, ϕ_t) defined in the DI frame. The x, z^{IM} axis of the IM frame are in the imaging plane, while the y axis is perpendicular to the plane. The symmetry axis of the probe laser beam (z^{PR} axis of the PR frame) is at polar angles $(\theta'_p, \pi/2)$ in the IM frame (not shown). (a) The polarization direction of dissociation laser (\mathbf{E}_{diss}) is along the z^{IM} axis of the IM frame and (b) the polarization direction of dissociation laser (\mathbf{E}_{diss}) is along the y axis of IM frame.

D. Signal intensity in 2D experiments

For calculation of the 2D images, we define an *imaging* frame (IM) by choosing the y axis perpendicular to the image plane and the x and z^{IM} in the plane. In ordinary experimental conditions, the width of the time-of-flight distribution for one particular ionic species (m/e) is negligible, $\Delta T_{\text{tot}}/T_{\text{tot}} \ll 1$. Then, the signal intensity $N(\tilde{x}_i, \tilde{z}_j)$ is expressed by the following formula:

$$\begin{aligned} N(\tilde{x}_i, \tilde{z}_j) &= c \int_{x_i}^{x_{i+1}} dx \int_{z_j}^{z_{j+1}} dz \int \frac{1}{v_t(x, y, z)} f(E_t(x, y, z)) \\ &\quad \times I(\theta_t(x, y, z), \phi_t(x, y, z)) dy, \end{aligned} \quad (34)$$

where $(\tilde{x}_i, \tilde{z}_j)$ represent the position of the pixel in 2D plane. (x_i, x_{i+1}) and (z_j, z_{j+1}) describe the size of the pixel. $f(E_t(x, y, z))$ is the translational energy distribution and v_t is the recoil velocity of the fragments in the center-of-mass (c.m.) frame. $(\theta_t(x, y, z), \phi_t(x, y, z))$ are the polar angles of v_t in the DI frame. $I(\theta_t(x, y, z), \phi_t(x, y, z))$ is identical with the one in Eqs. (23a) or (23b). We have assumed that the multipole moments are independent of $f(E_t(x, y, z))$. A detailed explanation of the above formula can be found in Appendix D.

When the z^{PR} axis (PR frame) is parallel to the Z^{DI} axis (DI frame), $I(\theta_t(x, y, z), \phi_t(x, y, z))$ can be calculated according to Eq. (23b) without the consideration of ϕ_t . In other cases, ϕ_t must be taken into account. We use the convention that the z^{PR} axis is in the XZ plane of the DI frame (Fig. 1).

In the present work, we have observed images with the polarization direction of the dissociation laser either parallel or perpendicular to the image plane and the z^{PR} axis is at the polar angles $(\theta'_p, \pi/2)$ in the IM frame. When the Z^{DI} axis is along the z^{IM} axis of the IM frame [configuration (a) in Fig. 2], the polar angles of velocity and the z^{PR} axis in the DI frame are given by

$$\cos \theta_t = \frac{v_z}{\sqrt{v_x^2 + v_y^2 + v_z^2}}, \quad \tan \phi_t = \frac{v_x}{v_y}, \quad (35a)$$

$$\theta_p = \theta'_p, \quad \phi_p = 0. \quad (35b)$$

When the Z^{DI} axis is along the y axis of the IM frame [configuration (b) in Fig. 2], we have

$$\cos \theta_t = \frac{v_y}{\sqrt{v_x^2 + v_y^2 + v_z^2}}, \quad \tan \phi_t = \frac{v_x}{v_z}, \quad (36a)$$

$$\theta_p = \frac{\pi}{2} - \theta'_p, \quad 0 \leq \theta'_p \leq \frac{\pi}{2}, \quad \phi_p = 0. \quad (36b)$$

From Eqs. (35a)–(36b), v_x , v_y , and v_z represent the projection of v_t on the x , y and z^{IM} axes of the IM frame, respectively.

IV. APPLICATION TO PHOTODISSOCIATION OF NO₂ AT 355 nm

A. Geometrical factors for the Q branch of NO(*C*²Π) ←←NO(*X*²Π)

As shown in Sec. III B 3, when $J_i = J_f$ and $\Lambda_i = \Lambda_f$, we need to know the ratio of $[G(\Lambda_i - 1) + G(\Lambda_i + 1)] : G(\Lambda_i) = \perp : \parallel$ to calculate the geometrical factors $P_0 : P_2 : P_4$. In the present case, the following ratio has been obtained from the two-photon laser-induced fluorescence (LIF) spectroscopy of NO reported previously²⁶

$$\perp : \parallel = 1.0 : 0.22 \sim 0.0. \quad (37)$$

From the oscillator strengths reported for one-photon transitions,³⁸ the following ratio is also deduced

$$\perp : \parallel = 1.0 : 0.14, \quad (38)$$

which is in reasonable agreement with Eq. (37).

It should be noted, however, that the LIF intensity is possibly affected by predissociation in the *C* state which leads to an error in the estimation. In this sense, [2 + 1] REMPI spectroscopy is expected to provide more accurate estimation than two-photon LIF. We have simulated the [2 + 1] REMPI spectra of NO at room temperature measured by Hippler and Pfab,^{30,39} and found the following ratio:

$$\perp : \parallel = 1.0 : 0.2 (\pm 0.1). \quad (39)$$

On the other hand, simulation of 2D images provided the following ratio as the best-fit parameter to the experimental data:

$$\perp : \parallel = 1.0 : 0.3. \quad (40)$$

Equation (40) provides the following geometrical factors [from Eqs. (11a), (13), and (17)]:

$$P_0 : P_2 : P_4 = 1 : 0.94 : 0.18, \quad J_i = 30.5. \quad (41)$$

B. The μ - ν - \mathbf{J} vector correlation

We employed Dirac's δ functions to perform the averaging in Eqs. (25a) and (25b). The rotational temperature of NO₂ is extremely low in the molecular beam, so that the conservation of angular momentum requires the angular momentum of NO to be perpendicular to its recoil direction ($\nu \perp \mathbf{J}$) for high \mathbf{J} . We assume that the angle between ν and absorption dipole moment μ is $41^\circ (\pm 3^\circ)$ or a bond angle of $98^\circ (\pm 6^\circ)$ that provides anisotropy parameter β of 0.71

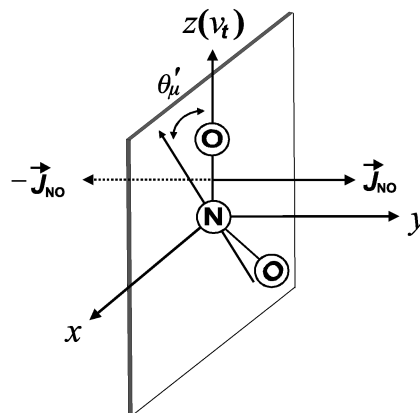


FIG. 3. Relation of coordinates in the VF frame employed for calculating the multipole moments of NO in 355 nm photodissociation of NO₂. The molecule is in the xz plane. The angular momentum (\mathbf{J}) of NO is either at y or $-y$ direction, or distributed equally between them (see the discussions in Sec. IV B). The angle between the direction of recoil velocity (ν) and transition dipole moment (μ) is $41^\circ (\pm 3^\circ)$. μ is in the molecular plane.

(± 0.15). These assumptions provide a fixed μ - ν - \mathbf{J} triple vector correlation (Fig. 3) except the sign of ϕ'_j .

For linearly polarized probe light, only even ranks of multipole moments contribute to the absorption intensity. From the comparison of Eqs. (25a), (25b), (29a), and (29b), it is easy to see that in the case of $\nu \perp \mathbf{J}$ and $\mu \perp \mathbf{J}$ in the VF frame, we have

$$g_k = \tilde{g}_k, \quad k \text{ even}, \quad (42a)$$

$$g(k, q) = \tilde{g}(k, q), \quad k \text{ even}. \quad (42b)$$

It means that using linearly polarized light the following limiting cases cannot be distinguished, e.g., (1) ϕ'_j is positive, (2) ϕ'_j is negative, and (3) the positive and negative values of ϕ'_j are equally probable.

The 355 nm photodissociation of NO₂ produces three spin-orbit states of O(³P₂), O(³P₁), and O(³P₀), therefore, NO(²Π_{1/2}, $J = 30.5, f$) have three different speeds of, 632, 596, and 578 (m/s) in the center of mass frame, respectively. The overall branching ratios have been reported to be O(³P₂):O(³P₁):O(³P₀) = 1:0.19:0.03.^{22,25} Although the ratios of O(³P_{*j*}) corresponding to NO(²Π_{1/2}, $J = 30.5, f$) could be different from the above values, we used these branching ratios in the simulation, since its effect is only minor. We have also taken into account the limited spatial resolution of our imaging apparatus. Depolarization of multipole moments by nuclear spins are neglected, because of the large angular momentum of NO.³⁴

In the simulation, 5, 5, and 200 points have been used for the x , z , and y directions in Eq. (34), respectively. The images calculated for $6 \times 6 \times 300$ points were the same. The width of the three energy components of NO corresponding to O(³P_{*j*}) counterparts were assumed to be 0.4 kJ/mol. The simulation of each image took 15–70 min with an IBM RS/6000 workstation (model 390).

In Figs. 4(A)–4(D) are the experimental images, and Figs. 4(a)–4(d) are the corresponding simulation by using a forward convolution method. The sizes of the images are 200×200 pixels for Figs. 4(A)–4(C), while 150

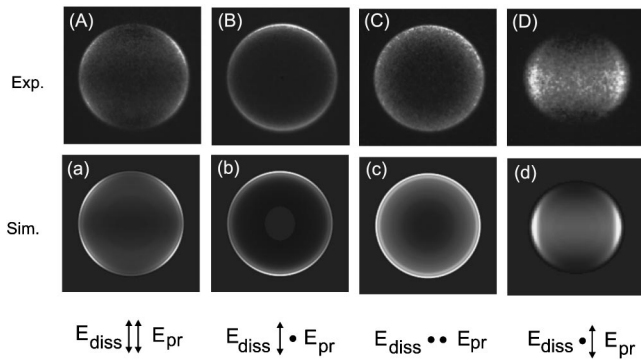


FIG. 4. 2D ion images of $\text{NO}(X^2\Pi_{1/2}, \nu=0, J=30.5, f)$ produced by 355 nm photodissociation of NO_2 measured with different pump-probe polarization configurations. The $[2+1]$ REMPI via $C(^2\Pi)$ state with $Q_{y1f}(30.5)$ line has been employed. (A)–(D) are the experimental data, and (a)–(d) are the simulations.

$\times 150$ pixels for Fig. 4(D). The polarization directions of the dissociation and probe laser beams are also shown in Fig. 4. The good agreement between the experimental and the simulated images demonstrates the validity of our theoretical treatment.

The pattern of the images can be explained as follows. For the Q line, the geometrical factors P_2 and P_4 are positive [see Eq. (41)], so that \mathbf{J} parallel to the probe laser polarization (\mathbf{E}_{pr}) is favored in probing. On the other hand, ν tends to be parallel to the polarization direction of the dissociation laser (\mathbf{E}_{diss}) because of the positive β value. Therefore, for $\mathbf{E}_{\text{diss}} // \mathbf{E}_{\text{pr}}$, the fragments scattered along the \mathbf{E}_{diss} cannot be detected efficiently because of $\mathbf{J} \perp \nu // \mathbf{E}_{\text{pr}}$ [Figs. 4(A) and 4(C)]. However, for $\mathbf{E}_{\text{diss}} \perp \mathbf{E}_{\text{pr}}$, the intensity along the \mathbf{E}_{diss} is increased [Figs. 4(B) and 4(D)].

In order to ascertain the anisotropy parameter β free from the ν - \mathbf{J} correlation, the image of $\text{O}(^3P_0)$ shown in Fig. 5 was analyzed. By using Abel transform, the translational energy distribution and $\beta(E_t)$ were obtained. It was found that β depends strongly on the translational energy. The center of mass (c.m.) translation energy release in producing $\text{O}(^3P_0)$ and $\text{NO}(X^2\Pi_{1/2}, j=30.5)$ is 1209 cm^{-1} . The average value of β for the c.m. translation energy release be-

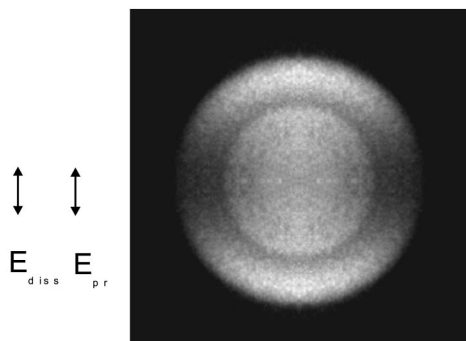


FIG. 5. Symmetrized 2D ion image of $\text{O}(^3P_0)$ produced by 355 nm photodissociation of NO_2 . The polarization directions of the dissociation laser and the probe laser are vertical in the plane. The size of image is 400×400 pixels.

tween 1170 and 1400 cm^{-1} was $0.73 (\pm 0.2)$, in excellent agreement with $0.71 (\pm 0.15)$ obtained from the $\text{NO}(X^2\Pi_{1/2}, j=30.5)$ images.

V. CONCLUSIONS

We presented the semiclassical formalism to analyze 3D [Eqs. (23a) and (23b)] and 2D [Eq. (34)] imaging data by including vector correlation. The geometrical factors P_k for the two-photon absorption of diatomic molecules have been presented for the intermediate coupling between Hund's case (a) and (b) [Eqs. (11a)–(11d)]. For linearly polarized light with $J_i=J_f$ and $\Lambda_i=\Lambda_f$, the geometrical factors depend on the relative ratio of different transition pathways. However, the factors are independent of the coupling cases for high J and given by simple formulas [Eqs. (16) and (17)]. The semiclassical treatment of angular momentum polarization has been critically tested by comparing with the experimental data on NO from 355 nm photodissociation of NO_2 . Good agreement between theory and experiment demonstrates the validity of our treatment.

ACKNOWLEDGMENTS

Y.M. thanks Japan Society for the Promotion of Science (JSPS) for a postdoctoral fellowship. Financial support from the Ministry of Education, Science, Sports and Culture (Contract Nos. 08559014 and 09440208) and the New Energy and Industrial Technology Development Organization are gratefully acknowledged.

APPENDIX A

In this Appendix we derive the geometrical factors for two-photon absorption of diatomic molecules in the intermediate coupling between Hund's case (a) and (b).

We first assume that the electronic state, $^{2S+1}\Sigma_0^\pm$, is not involved in the transition. We use the following conventions: (1) Λ_f is larger than or equal to zero, and (2) if $\Lambda_f=0$, Ω_f is larger than zero. The symmetric basis function of Hund's case (a) has the following form:

$$\psi(^{2S+1}\Lambda_{\Omega=\Sigma+\Lambda})_f = \frac{1}{\sqrt{2}} (|n_f \Lambda_f S \Sigma_f J_f M_f \Omega_f\rangle + a_{p_f} |n_f - \Lambda_f S - \Sigma_f J_f M_f - \Omega_f\rangle), \quad (\text{A1a})$$

where³³

$$\begin{aligned} |n_f \Lambda_f S \Sigma_f J_f M_f \Omega_f\rangle &= |n_f \Lambda_f S \Sigma_f\rangle |J_f M_f \Omega_f\rangle \\ &= \sqrt{\frac{2J_f+1}{8\pi^2}} D_{M_f \Omega_f}^{(J_f)*}(\alpha, \beta, \gamma) |n_f \Lambda_f S \Sigma_f\rangle. \end{aligned} \quad (\text{A1b})$$

$$a_{p_f} = \pm 1, \quad \pm \text{depends on the parity of the state.}$$

$$(\text{A1c})$$

The wave function for the virtual states can also be written as

$$\begin{aligned} \psi(^{2S+1}\Lambda_{\Omega=\Sigma+\Lambda})_e &= \frac{1}{\sqrt{2}} (|n_e\Lambda_e S\Sigma_e J_e M_e \Omega_e\rangle \\ &+ a_{p_e} |n_e - \Lambda_e S - \Sigma_e J_e M_e - \Omega_e\rangle). \end{aligned} \quad (\text{A2})$$

Assuming that i_{sp} is a space inversion operator, we obtain

$$i_{sp} r i_{sp} = -r, \quad (\text{A3})$$

$$\begin{aligned} i_{sp} |n_f \Lambda_f S \Sigma_f J_f M_f \Omega_f\rangle \\ = (-1)^{J_f - S + s_f} |n_f - \Lambda_f S - \Sigma_f M_f - \Omega_f\rangle, \end{aligned} \quad (\text{A4})$$

where $s_f = 1$ for Σ^- states, $s_f = 0$ for all other states.³³

Using Eqs. (A3) and (A4), the dipole matrix element between two Hund's case (a) basis can be expanded as

$$\begin{aligned} \langle \psi(^{2S+1}\Lambda_{\Omega=\Sigma+\Lambda})_f | \vec{r} \cdot \hat{\epsilon} | \psi(^{2S+1}\Lambda_{\Omega=\Sigma+\Lambda})_e \rangle \\ = \frac{1}{2} (1 + a_{p_f} a_{p_e} (-1)^{J_f + J_e - 2S + 1 + s_f + s_e}) \\ \times \langle n_f \Lambda_f S \Sigma_f J_f M_f \Omega_f | \vec{r} \cdot \hat{\epsilon} | n_e \Lambda_e S \Sigma_e J_e M_e \Omega_e \rangle. \end{aligned} \quad (\text{A5})$$

In deriving the above formula we assumed that the projection Σ of spin S onto the molecular axis does not change in the dipole absorption process for Hund's case (a).

The two-photon absorption intensity is evaluated from the following product of two matrix elements:

$$\begin{aligned} \sum_{a_{p_e}} \langle \psi(^{2S+1}\Lambda_{\Omega=\Sigma+\Lambda})_f | \vec{r} \cdot \hat{\epsilon} | \psi(^{2S+1}\Lambda_{\Omega=\Sigma+\Lambda})_e \rangle \langle \psi(^{2S+1}\Lambda_{\Omega=\Sigma+\Lambda})_e | \vec{r} \cdot \hat{\epsilon} | \psi(^{2S+1}\Lambda_{\Omega=\Sigma+\Lambda})_i \rangle \\ = \langle n_f \Lambda_f S \Sigma_f J_f M_f \Omega_f | \vec{r} \cdot \hat{\epsilon} | n_e \Lambda_e S \Sigma_e J_e M_e \Omega_e \rangle \langle n_e \Lambda_e S \Sigma_e J_e M_e \Omega_e | \vec{r} \cdot \hat{\epsilon} | n_i \Lambda_i S \Sigma_i J_i M_i \Omega_i \rangle. \end{aligned} \quad (\text{A9})$$

For a diatomic molecule in the intermediate coupling between Hund's cases (a) and (b), the wave function can be expanded by Hund's case (a) basis [see Eqs. (10a) and (10b) in the main text]. Therefore, two-photon absorption strength is expanded as follows:

$$\begin{aligned} \left| \sum_{\psi_e} \frac{\langle \Psi_f | \vec{r} \cdot \hat{\epsilon} | \psi_e \rangle \langle \psi_e | \vec{r} \cdot \hat{\epsilon} | \Psi_i \rangle}{E_e - E_i - i\Gamma_e/2 - h\nu} \right|^2 \\ = \sum_{\Omega_i \Omega_f n_e \Lambda_e J_e M_e \Omega_e \tilde{\Omega}_e} C_{\Omega_f}^{(f)*} C_{\Omega_i}^{(i)} C_{\Omega_e} (C_{\tilde{\Omega}_e})^* \\ \times \frac{\langle n_f \Lambda_f S \Sigma_f J_f M_f \Omega_f | \vec{r} \cdot \hat{\epsilon} | n_e \Lambda_e S \Sigma_e J_e M_e \Omega_e \rangle \langle n_e \Lambda_e S \Sigma_e J_e M_e \tilde{\Omega}_e | \vec{r} \cdot \hat{\epsilon} | n_i \Lambda_i S \Sigma_i J_i M_i \Omega_i \rangle}{E_{n_e \Lambda_e J_e} - E_i - i\Gamma_{n_e \Lambda_e J_e}/2 - h\nu} \\ \times \sum_{\Omega'_f \Omega'_i n'_e \Lambda'_e J'_e M'_e \Omega'_e \tilde{\Omega}'_e} \left(C_{\Omega'_f}^{(f)*} C_{\Omega'_i}^{(i)} C_{\Omega'_e} (C_{\tilde{\Omega}'_e})^* \right. \\ \left. \times \frac{\langle n_f \Lambda_f S \Sigma'_f J'_f M'_f \Omega'_f | \vec{r} \cdot \hat{\epsilon} | n'_e \Lambda'_e S \Sigma'_e J'_e M'_e \Omega'_e \rangle \langle n'_e \Lambda'_e S \Sigma'_e J'_e M'_e \tilde{\Omega}'_e | \vec{r} \cdot \hat{\epsilon} | n_i \Lambda_i S \Sigma'_i J'_i M'_i \Omega'_i \rangle}{E_{n'_e \Lambda'_e J'_e} - E_i - i\Gamma_{n'_e \Lambda'_e J'_e}/2 - h\nu} \right). \end{aligned} \quad (\text{A10})$$

In Eq. (A10) we used C_{Ω_e} to represent the expansion coefficients for the virtual states.

The geometrical factor P_k can be calculated by using Eq. (9) in the main text,

$$\begin{aligned} \sum_{a_{p_e}} \langle \psi(^{2S+1}\Lambda_{\Omega=\Sigma+\Lambda})_f | \vec{r} \cdot \hat{\epsilon} | \psi(^{2S+1}\Lambda_{\Omega=\Sigma+\Lambda})_e \rangle \\ \times \langle \psi(^{2S+1}\Lambda_{\Omega=\Sigma+\Lambda})_e | \vec{r} \cdot \hat{\epsilon} | \psi(^{2S+1}\Lambda_{\Omega=\Sigma+\Lambda})_i \rangle \\ = \sum_{a_{p_e}} \frac{1}{4} (1 + a_{p_e} a_{p_f} (-1)^{J_f + J_e - 2S + 1 + s_e + s_f}) \\ \times (1 + a_{p_e} a_{p_i} (-1)^{J_i + J_e - 2S + 1 + s_e + s_i}) \\ \times \langle n_f \Lambda_f S \Sigma_f J_f M_f \Omega_f | \vec{r} \cdot \hat{\epsilon} | n_e \Lambda_e S \Sigma_e J_e M_e \Omega_e \rangle \\ \times \langle n_e \Lambda_e S \Sigma_e J_e M_e \Omega_e | \vec{r} \cdot \hat{\epsilon} | n_i \Lambda_i S \Sigma_i J_i M_i \Omega_i \rangle. \end{aligned} \quad (\text{A6})$$

For Eq. (A6) to be nonzero, the following condition must be fulfilled:

$$a_{p_f} (-1)^{J_f + J_e - 2S + 1 + s_e + s_f} = a_{p_i} (-1)^{J_e + J_i - 2S + 1 + s_e + s_i}$$

or equivalently,

$$a_{p_f} (-1)^{J_f + s_f} = a_{p_i} (-1)^{J_i + s_i}. \quad (\text{A7})$$

We have the following selection rules for Eq. (A6):

$$\begin{aligned} \Delta J = 0, \pm 2, \quad \text{allowed transitions } e-e, f-f, \\ \Delta J = \pm 1, \quad \text{allowed transitions } e-f, f-e. \end{aligned} \quad (\text{A8})$$

It is easily seen that there is only one a_{p_e} value, which makes Eq. (A6) to be nonzero. Thus, the summation is reduced to one term:

$$\begin{aligned}
P_k &= \sum_{M_i M_f} \left| \sum_{\psi_e} \frac{\langle \Psi_f | \vec{r} \cdot \hat{\epsilon} | \psi_e \rangle \langle \psi_e | \vec{r} \cdot \hat{\epsilon} | \Psi_i \rangle}{E_e - E_i - i\Gamma_e/2 - h\nu} \right|^2 (-1)^{J_i - M_i} \sqrt{2k+1} \begin{pmatrix} J_i & k & J_i \\ -M_i & 0 & M_i \end{pmatrix} \\
&= \sum_{\Omega_f \Omega'_f \Omega_i \Omega'_i} C_{\Omega_f}^{(f)*} C_{\Omega_i}^{(i)} (C_{\Omega'_f}^{(f)*} C_{\Omega'_i}^{(i)})^* P_k(\Omega_f, \Omega_i, \Omega'_f, \Omega'_i), \tag{A11}
\end{aligned}$$

where

$$\begin{aligned}
&P_k(\Omega_f, \Omega_i, \Omega'_f, \Omega'_i) \\
&= \sum_{M_i M_f} (-1)^{J_i - M_i} \begin{pmatrix} J & k & J \\ -M_i & 0 & M_i \end{pmatrix} \sum_{n_e \Lambda_e J_e M_e \Omega_e \bar{\Omega}_e} C_{\Omega_e} (C_{\bar{\Omega}_e})^* \\
&\quad \times \frac{\langle n_f \Lambda_f S \Sigma_f J_f M_f \Omega_f | \vec{r} \cdot \hat{\epsilon} | n_e \Lambda_e S \Sigma_f J_e M_e \Omega_e \rangle \langle n_e \Lambda_e S \Sigma_i J_e M_e \bar{\Omega}_e | \vec{r} \cdot \hat{\epsilon} | n_i \Lambda_i S \Sigma_i J_i M_i \Omega_i \rangle}{E_{n_e \Lambda_e J_e} - E_i - i\Gamma_{n_e \Lambda_e J_e}/2 - h\nu} \\
&\quad \times \left(\sum_{n'_e \Lambda'_e J'_e M'_e \Omega'_e \bar{\Omega}'_e} C_{\Omega'_e} (C_{\bar{\Omega}'_e})^* \frac{\langle n_f \Lambda_f S \Sigma'_f J_f M_f \Omega_f | \vec{r} \cdot \hat{\epsilon} | n'_e \Lambda'_e S \Sigma'_f J'_e M'_e \Omega'_e \rangle \langle n'_e \Lambda'_e S \Sigma'_i J'_e M'_e \bar{\Omega}'_e | \vec{r} \cdot \hat{\epsilon} | n_i \Lambda_i S \Sigma'_i J_i M_i \Omega_i \rangle}{E_{n'_e \Lambda'_e J'_e} - E_i - i\Gamma_{n'_e \Lambda'_e J'_e}/2 - h\nu} \right)^*. \tag{A12}
\end{aligned}$$

In order to facilitate the integration, we employ the *body-fixed* frame (BF):

$$\vec{r} \cdot \hat{\epsilon} = (-1)^s \epsilon_{-s}^{(1)} r_s^{(1)} (\text{PR}) = (-1)^s \epsilon_{-s}^{(1)} \sum_{q_1} D_{sq_1}^{(1)*}(\alpha, \beta, \gamma) r_{q_1}^{(1)} (\text{BF}). \tag{A13}$$

We have

$$\begin{aligned}
&\sum_{n_e \Lambda_e J_e M_e \Omega_e \bar{\Omega}_e} C_{\Omega_e} (C_{\bar{\Omega}_e})^* \frac{\langle n_f \Lambda_f S \Sigma_f J_f M_f \Omega_f | \vec{r} \cdot \hat{\epsilon} | n_e \Lambda_e S \Sigma_f J_e M_e \Omega_e \rangle \langle n_e \Lambda_e S \Sigma_i J_e M_e \bar{\Omega}_e | \vec{r} \cdot \hat{\epsilon} | n_i \Lambda_i S \Sigma_i J_i M_i \Omega_i \rangle}{E_{n_e \Lambda_e J_e} - E_i - i\Gamma_{n_e \Lambda_e J_e}/2 - h\nu} \\
&= \sum_{J_e M_e \Omega_e \bar{\Omega}_e} \sum_{q_1 q_2 n_e \Lambda_e} \frac{\langle n_f \Lambda_f S \Sigma_f | r_{q_1}^{(1)} | n_e \Lambda_e S \Sigma_f \rangle \langle n_e \Lambda_e S \Sigma_i | r_{q_2}^{(1)} | n_i \Lambda_i S \Sigma_i \rangle}{E_{n_e \Lambda_e J_e} - E_i - i\Gamma_{n_e \Lambda_e J_e}/2 - h\nu} \\
&\quad \times C_{\Omega_e} (C_{\bar{\Omega}_e})^* \langle J_f M_f \Omega_f | D_{sq_1}^{(1)*} | J_e M_e \Omega_e \rangle \langle J_e M_e \bar{\Omega}_e | D_{sq_2}^{(1)*} | J_i M_i \Omega_i \rangle. \tag{A14}
\end{aligned}$$

We assume that the transition dipole moment is independent of the projection Λ of the spin S onto the diatomic axis. We have

$$\begin{aligned}
&\langle n_f \Lambda_f S \Sigma_f | r_{q_1}^{(1)} | n_e \Lambda_e S \Sigma_f \rangle \langle n_e \Lambda_e S \Sigma_i | r_{q_2}^{(1)} | n_i \Lambda_i S \Sigma_i \rangle \\
&= \langle n_f \Lambda_f S \Sigma_f | r_{q_1}^{(1)} | n_e \Lambda_e S \Sigma_f \rangle \langle n_e \Lambda_e S \Sigma_i | r_{q_2}^{(1)} | n_i \Lambda_i S \Sigma_i \rangle. \tag{A15}
\end{aligned}$$

We neglect the energy differences due to the rotational quantum numbers in the intermediate states, since these are small in comparing with the energy differences due to different electronic configurations.³⁴ We define a complete basis set $|J_e M_e\rangle$,

$$|J_e M_e\rangle = \sum_{\Omega_e} C_{\Omega_e} |J_e M_e \Omega_e\rangle. \tag{A16a}$$

Using the closure relation, we obtain⁴⁰

$$\begin{aligned}
\sum_{J_e M_e} |J_e M_e\rangle \langle J_e M_e| &= \sum_{J_e M_e \Omega_e \bar{\Omega}_e} C_{\Omega_e} (C_{\bar{\Omega}_e})^* |J_e M_e \Omega_e\rangle \\
&\quad \times \langle J_e M_e \bar{\Omega}_e| = I, \tag{A16b}
\end{aligned}$$

where I is the unit operator. Also by noting the property of rotation matrices,³¹

$$\begin{aligned}
&D_{sq_1}^{(1)*}(\alpha, \beta, \gamma) D_{sq_2}^{(1)*}(\alpha, \beta, \gamma) \\
&= \sum_R (2R+1) \begin{pmatrix} 1 & 1 & R \\ s & s & -2s \end{pmatrix} \begin{pmatrix} 1 & 1 & R \\ q_1 & q_2 & r \end{pmatrix} \\
&\quad \times D_{-2s, r}^{(R)}(\alpha, \beta, \gamma). \tag{A17}
\end{aligned}$$

Equation (A14) can be thus simplified to:

$$\begin{aligned}
 & \sum_{q_1 q_2} \left(\sum_{n_e \Lambda_e} \frac{\langle n_f \Lambda_f S \Sigma | r_{q_1}^{(1)} | n_e \Lambda_e S \Sigma \rangle \langle n_e \Lambda_e S \Sigma | r_{q_2}^{(1)} | n_i \Lambda_i S \Sigma \rangle}{E_{n_e \Lambda_e} - E_i - i\Gamma_{n_e \Lambda_e} / 2 - h\nu} \right) \sum_R \langle D_{M_f \Omega_f}^{(J_f)*} | D_{-2s, r}^{(R)} | D_{M_i \Omega_i}^{(J_i)*} \rangle \\
 & \times (2R+1) \begin{pmatrix} 1 & 1 & R \\ s & s & -2s \end{pmatrix} \begin{pmatrix} 1 & 1 & R \\ q_1 & q_2 & r \end{pmatrix} \sqrt{\frac{(2J_f+1)(2J_i+1)}{(8\pi^2)^2}} \\
 & = \sum_R \left[\sum_{n_e \Lambda_e} \frac{\langle n_f \Lambda_f S \Sigma | r_{\Lambda_f - \Lambda_e}^{(1)} | n_e \Lambda_e S \Sigma \rangle \langle n_e \Lambda_e S \Sigma | r_{\Lambda_e - \Lambda_i}^{(1)} | n_i \Lambda_i S \Sigma \rangle}{E_{n_e \Lambda_e} - E_i - i\Gamma_{n_e \Lambda_e} / 2 - h\nu} \begin{pmatrix} 1 & 1 & R \\ \Lambda_f - \Lambda_e & \Lambda_e - \Lambda_i & \Lambda_i - \Lambda_f \end{pmatrix} \begin{pmatrix} 1 & 1 & R \\ s & s & -2s \end{pmatrix} \right] \\
 & \times (-1)^{M_i - \Omega_i} \begin{pmatrix} J_i & R & J_f \\ -M_i & -2s & M_f \end{pmatrix} \begin{pmatrix} J_i & R & J_f \\ -\Omega_i & r & \Omega_f \end{pmatrix} \sqrt{(2J_i+1)(2J_f+1)(2R+1)} \\
 & = \sum_R \sum_{\Lambda_e} G(\Lambda_e) \begin{pmatrix} 1 & 1 & R \\ \Lambda_f - \Lambda_e & \Lambda_e - \Lambda_i & \Lambda_i - \Lambda_f \end{pmatrix} \begin{pmatrix} 1 & 1 & R \\ s & s & -2s \end{pmatrix} \\
 & \times (-1)^{M_i - \Omega_i} \begin{pmatrix} J_i & R & J_f \\ -M_i & -2s & M_f \end{pmatrix} \begin{pmatrix} J_i & R & J_f \\ -\Omega_i & \Omega_i - \Omega_f & \Omega_f \end{pmatrix} \sqrt{(2J_i+1)(2J_f+1)(2R+1)}. \tag{A18}
 \end{aligned}$$

Using Eq. (A18), we can simplify Eq. (A12) as follows:

$$\begin{aligned}
 & P_k(\Omega_f, \Omega_i, \Omega'_f, \Omega'_i) \\
 & = \sum_{RT \Lambda_e \Lambda'_e} G(\Lambda_e) G^*(\Lambda'_e) \begin{pmatrix} 1 & 1 & R \\ s & s & -2s \end{pmatrix} \begin{pmatrix} 1 & 1 & T \\ s & s & -2s \end{pmatrix} (2R+1)(2T+1) \begin{pmatrix} 1 & 1 & R \\ \Lambda_f - \Lambda_e & \Lambda_e - \Lambda_i & \Lambda_i - \Lambda_f \end{pmatrix} \\
 & \times \begin{pmatrix} 1 & 1 & T \\ \Lambda_f - \Lambda'_e & \Lambda'_e - \Lambda_i & \Lambda_i - \Lambda_f \end{pmatrix} (2J_i+1)(2J_f+1) \begin{pmatrix} J_i & R & J_f \\ -\Omega_i & \Omega_i - \Omega_f & \Omega_f \end{pmatrix} \begin{pmatrix} J_i & T & J_f \\ -\Omega'_i & \Omega'_i - \Omega'_f & \Omega'_f \end{pmatrix} \\
 & \times \sum_{M_i M_f} (-1)^{M_i - \Omega_i + M_i - \Omega'_i} (-1)^{J_i - M_i} \sqrt{2k+1} \begin{pmatrix} J_i & k & J_i \\ -M_i & 0 & M_i \end{pmatrix} \begin{pmatrix} J_i & R & J_f \\ -M_i & -2s & M_f \end{pmatrix} \begin{pmatrix} J_i & T & J_f \\ -M_i & -2s & M_f \end{pmatrix}. \tag{A19}
 \end{aligned}$$

The summation of M in Eq. (A19) can be performed using the following equation:³³

$$\begin{aligned}
 & \begin{Bmatrix} j_1 & j_2 & j_3 \\ j_4 & j_5 & j_6 \end{Bmatrix} \begin{pmatrix} j_5 & j_1 & j_6 \\ m_5 & m_1 & m_6 \end{pmatrix} \\
 & = \sum_{m_2, m_3, m_4} (-1)^{j_1 + j_2 - j_3 + j_4 + j_5 + j_6 - m_1 - m_4} \\
 & \times \begin{pmatrix} j_1 & j_2 & j_3 \\ m_1 & m_2 & -m_3 \end{pmatrix} \begin{pmatrix} j_4 & j_5 & j_6 \\ m_4 & m_5 & m_3 \end{pmatrix} \\
 & \times \begin{pmatrix} j_2 & j_4 & j_6 \\ m_2 & m_4 & -m_6 \end{pmatrix}. \tag{A20}
 \end{aligned}$$

Thus we obtain Eqs. (11a)–(11d) in the text. Finally, the assumption that there is no $^{2S+1}\Sigma_0$ state involved in the transition can be removed by applying the following rules in the calculation,

- (1) For pathway including the transition $^{2S+1}\Sigma_0 - ^{2S+1}\Pi_1$, $G(\Lambda_e)$ should be multiplied by a factor of $\sqrt{2}$. For ex-

ample, if a pathway is $^{2S+1}\Pi_1 - ^{2S+1}\Sigma_0 - ^{2S+1}\Pi_1$, $G(\Lambda_e)$ for *this pathway* should be replaced by: $\sqrt{2} \times \sqrt{2} G(0)$.

- (2) However, for a pathway including the transition $^{2S+1}\Sigma_0 - ^{2S+1}\Sigma_0$, no change is required.

APPENDIX B

From the definition of the expansion coefficients,¹³ we have

$$\begin{aligned}
 g(k, -q_2) & = \langle T_{kq_2}^+ (\text{VF}) C_{2-q_2}^* (\theta'_\mu, \phi'_\mu) \rangle_{J'\mu'} \\
 & = \langle T_{k-q_2}^+ (\text{VF}) C_{2q_2}^* (\theta'_\mu, \phi'_\mu) \rangle_{J'\mu'} = g^*(k, q_2). \tag{B1}
 \end{aligned}$$

where $T_{kq_2}^+ (\text{VF})$ is the state multipole in the VF frame.

The multipole moment $\rho_{-q}^{(k)}(\theta_t, \phi_t)$ is

$$\begin{aligned} \rho_{-q}^{(k)}(\theta_t, \phi_t) &= \frac{1}{4\pi} \left(g_k C_{k-q}^*(\theta_t, \phi_t) + 2 \sum_{q_2} g(k, q_2) \right. \\ &\quad \left. \times D_{-q-q_2}^{(k)}(\phi_t, \theta_t, 0) D_{0q_2}^{(2)}(\phi_t, \theta_t, 0) \right). \end{aligned} \quad (\text{B2})$$

We transform the second term in the above equation,

$$\begin{aligned} \sum_{q_2} g(k, q_2) D_{-q-q_2}^{(k)}(\phi_t, \theta_t, 0) D_{0q_2}^{(2)}(\phi_t, \theta_t, 0) &= \sum_{q_2} g(k, -q_2) D_{-qq_2}^{(k)}(\phi_t, \theta_t, 0) D_{0-q_2}^{(2)}(\phi_t, \theta_t, 0) \\ &= (-1)^q \sum_{q_2} g^*(k, q_2) D_{q-q_2}^{(k)*}(\phi_t, \theta_t, 0) D_{0q_2}^{(2)*}(\phi_t, \theta_t, 0). \end{aligned} \quad (\text{B3})$$

Thus, we obtain Eq. (21)

$$\begin{aligned} \rho_{-q}^{(k)}(\theta_t, \phi_t) &= \frac{1}{4\pi} \left(g_k (-1)^q C_{kq}(\theta_t, \phi_t) + 2(-1)^q \right. \\ &\quad \left. \times \sum_{q_2} g^*(k, q_2) D_{q-q_2}^{(k)*}(\phi_t, \theta_t, 0) D_{0q_2}^{(2)*}(\phi_t, \theta_t, 0) \right) \\ &= (-1)^q \rho_q^{(k)*}(\theta_t, \phi_t). \end{aligned} \quad (\text{B4})$$

APPENDIX C

First we note that the unit vectors for the x , y , z coordinates can be expressed by modified spherical harmonics

$$z = C_{10}(\theta_J, \phi_J), \quad (\text{C1a})$$

$$x = -\frac{1}{\sqrt{2}} (C_{11}(\theta_J, \phi_J) - C_{1-1}(\theta_J, \phi_J)), \quad (\text{C1b})$$

$$y = \frac{i}{\sqrt{2}} (C_{11}(\theta_J, \phi_J) + C_{1-1}(\theta_J, \phi_J)), \quad (\text{C1c})$$

where (θ_J, ϕ_J) are polar angles of angular momentum in DI frame.

The projection of the transition dipole moment on the Z axis of the DI frame is related to the corresponding values in the VF frame at the Euler angles $(\phi_t, \theta_t, \chi_t)$

$$\begin{aligned} C_{10}(\theta_\mu, \phi_\mu) &= \sum_p C_{1p}(\theta'_\mu, \phi'_\mu) D_{0p}^{(1)*}(\phi_t, \theta_t, \chi_t) \\ &= \sum_p C_{1p}(\theta'_\mu, \phi'_\mu) d_{0p}^{(1)}(\theta_t) e^{ip\chi_t}. \end{aligned} \quad (\text{C2})$$

For Euler angles $(\phi_t, \pi - \theta_t, \chi_t^*)$, we have

$$\begin{aligned} C_{10}(\theta_\mu^*, \phi_\mu^*) &= \sum_p C_{1p}(\theta'_\mu, \phi'_\mu) D_{0p}^{(1)*}(\phi_t, \pi - \theta_t, \chi_t^*) \\ &= \sum_p C_{1p}(\theta'_\mu, \phi'_\mu) (-1)^{1+p} d_{0p}^{(1)}(\theta_t) e^{ip\chi_t^*}. \end{aligned} \quad (\text{C3})$$

For the excitation probabilities to be the same for VF frames $(\phi_t, \theta_t, \chi_t)$ and $(\phi_t, \pi - \theta_t, \chi_t^*)$ (the case of $\mu \parallel \nu$ is not considered here), it is required

$$(-1)^p e^{ip\chi_t^*} = e^{ip\chi_t} \quad \text{or} \quad \chi_t^* = \chi_t \pm \pi. \quad (\text{C4})$$

Therefore, the VF frame at Euler angles $(\phi_t, \theta_t, \chi_t)$ has the same excitation probability with the VF frame at Euler angles $(\phi_t, \pi - \theta_t, \chi_t \pm \pi)$. However, the absolute projection values of photofragment angular momentum onto the X and Y axis for these two frames are not equal in general. First we note that

$$\begin{aligned} C_{1q}(\theta_J, \phi_J) &= \sum_p C_{1p}(\theta'_J, \phi'_J) D_{qp}^{(1)*}(\phi_t, \theta_t, \chi_t) \\ &= \sum_p C_{1p}(\theta'_J, \phi'_J) e^{iq\phi_t} d_{qp}^{(1)}(\theta_t) e^{ip\chi_t}, \end{aligned} \quad (\text{C5a})$$

$$\begin{aligned} C_{1q}(\theta_J^*, \phi_J^*) &= \sum_p C_{1p}(\theta'_J, \phi'_J) D_{qp}^{(1)*}(\phi_t, \pi - \theta_t, \chi_t \pm \pi) \\ &= \sum_p C_{1p}(\theta'_J, \phi'_J) e^{iq\phi_t} (-1) d_{qp}^{(1)}(\theta_t) e^{ip\chi_t}. \end{aligned} \quad (\text{C5b})$$

Using Eqs. (C1c) and (C5a), the projection of J onto the Y axis for Euler angles $(\phi_t, \theta_t, \chi_t)$ is

$$\frac{i}{\sqrt{2}} \sum_p C_{1p}(\theta'_J, \phi'_J) e^{ip\chi_t} [e^{i\phi_t} d_{1p}^{(1)}(\theta_t) + e^{-i\phi_t} d_{-1p}^{(1)}(\theta_t)]. \quad (\text{C6a})$$

For Euler angles $(\phi_t, \pi - \theta_t, \chi_t \pm \pi)$, the projection of J onto the Y axis is

$$-\frac{i}{\sqrt{2}} \sum_p C_{1p}(\theta'_J, \phi'_J) e^{ip\chi_t} [e^{i\phi_t} d_{-1p}^{(1)}(\theta_t) + e^{-i\phi_t} d_{1p}^{(1)}(\theta_t)]. \quad (\text{C6b})$$

From comparison of Eqs. (C6a) and (C6b), it is clear that, except in the case of $\theta'_J = 0$, the absolute values of the projection of J onto the Y axis for the two VF frames are not equal. In the same way, it can be shown that the absolute values of the projection of J onto the X axis for the two frames are also not equal.

Similarly, it can be also shown that for two VF frames with Euler angles $(\phi_t, \theta_t, \chi_t)$ and $(2\pi - \phi_t, \theta_t, \chi_t)$, the absolute values of the projection of J onto the X and Y axis are not equal.

APPENDIX D

In this appendix, we provide the formula to calculate the signal intensity in 2D imaging by projecting the 3D intensity. The product ion density in space produced by REMPI, N , is described by the following formula,

$$N = c v_t f(E_t) I(\theta_t, \phi_t) dv_t d\Omega_t, \quad (\text{D1})$$

where v_t is the product recoil velocity in the center of mass (c.m.) frame, $f(E_t)$ is the product translational energy distribution,⁴¹ $I(\theta_t, \phi_t)$ is the product angular distribution with (θ_t, ϕ_t) the polar angles of v_t in the DI frame, and $d\Omega_t$ is the solid angle of v_t in the DI frame.

We employ the IM frame to calculate the images. We change the velocity variable in the above equation from *velocity* space to the *coordinate* space,

$$\begin{aligned} N &= c \frac{f(E_t)}{v_t} I(\theta_t, \phi_t) v_t^2 dv_t d\Omega_t \\ &= c \frac{f(E_t)}{v_t} I(\theta_t, \phi_t) v_{\text{lab}}^2 dv_{\text{lab}} d\Omega_{\text{lab}} \\ &= c \frac{f(E_t(x, y, z))}{v_t(x, y, z)} I(\theta_t, \phi_t) \frac{1}{T_{\text{tot}}^3} r_{\text{lab}}^2 dr_{\text{lab}} d\Omega_{\text{lab}} \\ &= c \frac{f(E_t(x, y, z))}{v_t(x, y, z)} I(\theta_t, \phi_t) \frac{1}{T_{\text{tot}}^3} (dx dy dz)_{\text{lab}}, \quad (\text{D2}) \end{aligned}$$

where T_{tot} is an ion time-of-flight that can be regarded as a constant for a particular mass. The second equation changes the variables from the c.m. to laboratory (lab) frame. The 2D number density, $N(x, z)$, can be calculated by a summation of the different y variables at time T_{tot} :

$$N(x, z) = \left(\frac{c}{T_{\text{tot}}^3} \right) \int \frac{f(E_t(x, y, z))}{v_t(x, y, z)} I(\theta_t(x, y, z), \phi_t(x, y, z)) dy. \quad (\text{D3})$$

Considering the finite size of the pixel in 2D image experiments, we obtain Eq. (34).

¹J. P. Simons, J. Phys. Chem. **91**, 5378 (1987).

²P. L. Houston, J. Phys. Chem. **91**, 5388 (1987).

³A. J. Orr-Ewing and R. N. Zare, Annu. Rev. Phys. Chem. **45**, 315 (1994).

⁴R. N. Dixon, J. Chem. Phys. **85**, 1866 (1986).

⁵G. E. Hall, N. Sivakumar, D. Chawla, P. L. Houston, and I. Burak, J. Chem. Phys. **88**, 3682 (1988).

⁶M. Mons and I. Dimicoli, J. Chem. Phys. **90**, 4037 (1989).

⁷R. Uberna, R. D. Hinchliffe, and J. I. Cline, J. Chem. Phys. **103**, 7934 (1995).

⁸R. J. Gordon and G. E. Hall, *Application of Doppler Spectroscopy to Photofragmentation*, in Advances in Chemical Physics Vol. XVCI, 1, edited by I. Prigogine and Stuart A. Rice.

⁹M. H. M. Janssen, D. H. Parker, G. O. Sitz, S. Stolte, and D. W. Chandler, J. Phys. Chem. **95**, 8007 (1991).

¹⁰A. G. Suits, R. L. Miller, L. S. Bontuyan, and P. L. Houston, J. Chem. Soc., Faraday Trans. **89**, 1443 (1993).

¹¹Y. Mo, H. Katayanagi, M. C. Heaven, and T. Suzuki, Phys. Rev. Lett. **77**, 830 (1996).

¹²A. S. Bracker, E. R. Wouters, A. G. Suits, Y. T. Lee, and O. S. Vasyutinskii, Phys. Rev. Lett. **80**, 1626 (1998).

¹³Y. Mo and T. Suzuki, J. Chem. Phys. **108**, 6780 (1998).

¹⁴L. D. A. Siebbeles, M. Glass-Maujean, O. S. Vasyutinskii, J. A. Beswick, and O. Roncero, J. Chem. Phys. **100**, 3610 (1994).

¹⁵H. L. Kim, M. A. Wickramaaratchi, X. Zheng, and G. E. Hall, J. Chem. Phys. **101**, 2033 (1994).

¹⁶M. Brouard, H. M. Lambert, J. Short, and J. P. Simons, J. Phys. Chem. **99**, 13571 (1995).

¹⁷A. J. Orr-Ewing, W. R. Simpson, T. P. Rakitzis, S. A. Kandel, and R. N. Zare, J. Chem. Phys. **106**, 5961 (1997).

¹⁸D. H. Parker and A. T. J. B. Eppink, J. Chem. Phys. **107**, 2357 (1997).

¹⁹T. Kinugawa and T. Arikawa, J. Chem. Phys. **96**, 4801 (1992).

²⁰K. Chen, Chem. Phys. Lett. **198**, 288 (1992).

²¹K. Tonokura and T. Suzuki, Chem. Phys. Lett. **224**, 1 (1994).

²²J. Miyawaki, T. Tsuchizawa, K. Yamanouchi, and S. Tsuchiya, Chem. Phys. Lett. **165**, 168 (1990).

²³(a) T. Suzuki, V. P. Hradil, S. A. Hewitt, P. L. Houston, and B. J. Whitaker, Chem. Phys. Lett. **187**, 257 (1991); (b) V. P. Hradil, T. Suzuki, S. A. Hewitt, P. L. Houston, and B. J. Whitaker, J. Chem. Phys. **99**, 4455 (1993).

²⁴S. A. Reid, D. C. Robie, and H. Reisler, J. Chem. Phys. **100**, 4256 (1994).

²⁵C. H. Hsieh, Y. S. Lee, A. Fujii, S. H. Lee, and K. Liu, Chem. Phys. Lett. **277**, 33 (1997).

²⁶P. A. Freedman, Can. J. Phys. **55**, 1387 (1977).

²⁷C. Amiot, R. Bacis, and G. Guelachvili, Can. J. Phys. **56**, 251 (1978).

²⁸C. Amiot and H. J. Verges, Phys. Scr. **25**, 302 (1982).

²⁹J. E. Murray, K. Yoshino, J. R. Esmond, W. H. Parkinson, Y. Sun, A. Dalgarno, A. P. Thorne, and G. Cox, J. Chem. Phys. **101**, 62 (1994).

³⁰M. Hippler and J. Pfab, Mol. Phys. **94**, 313 (1998).

³¹A. J. Bain and A. J. McCaffery, J. Chem. Phys. **83**, 2627 (1985); **83**, 2632 (1985); **83**, 2641 (1985).

³²K. Blum, *Density Matrix Theory and Applications* (Plenum, New York, 1981).

³³R. N. Zare, *Angular Momentum* (Wiley, New York, 1988).

³⁴A. C. Kummel, G. O. Sitz, and R. N. Zare, J. Chem. Phys. **85**, 6874 (1986).

³⁵M. P. Docker, Chem. Phys. **125**, 185 (1988).

³⁶(a) H. Meyer, Chem. Phys. Lett. **230**, 510 (1994); (b) H. Meyer, J. Chem. Phys. **107**, 7721 (1997).

³⁷Y. Mo and T. Suzuki, J. Chem. Phys. **109**, 4691 (1998).

³⁸P. Cremaschi, P. M. Johnson, and J. L. Whitten, J. Chem. Phys. **69**, 4341 (1978).

³⁹In the simulation, the Hönl-London factors, HL, for two-photon line strength were calculated by $HL = \sqrt{2J+1}P_0$. Because of the predissociation and perturbation in NO($B^2\Pi$) and NO($C^2\Pi$) states, a global fitting could not fully reproduce [2+1] REMPI spectra of Ref. 30.

⁴⁰K. Chen and E. S. Yeung, J. Chem. Phys. **69**, 43 (1978).

⁴¹Because there are some internal energy distributions in the molecular beam, we can always assume a translational energy distribution of photofragments, even if we probe diatomic molecules with state-resolved detection in the dissociation of triatomic molecules. If there were only one velocity component, the Jacobi transformation would be different from our discussions. See G. L. Catchen, J. Husain, and R. N. Zare, J. Chem. Phys. **69**, 1737 (1978).